

Phonon modes of magnetic vortex lattices in finite isospin QCD

Prabal Adhikari

Physics Department, Faculty of Natural Sciences and Mathematics, St. Olaf College, 1520 St. Olaf Avenue, Northfield, MN 55057, United States

Elizabeth Leeser, Jake Markowski

St. Olaf College, 1520 St. Olaf Avenue, Northfield, MN 55057, United States

Abstract

We study phonon modes associated with the magnetic vortex lattices in finite isospin chiral perturbation theory near the upper critical point by introducing quasimomentum fluctuations to the lattice and find the dispersion relations associated with the optical and acoustic modes. We find that one of the optical modes is massless and that its energy for small transverse quasimomentum is quintic (due to the presence of an isospin chemical potential), which is significantly softer than the “supersoft” (quadratic) massless mode of the Abelian Higgs Model (AHM). Unlike the AHM, the speed of the longitudinal mode depends on both the isospin chemical potential and the external magnetic field due to the presence of derivative interactions. Our results suggest that the finite isospin phase diagram of Quantum Chromodynamics supports a disordered (liquid/gas) phase of magnetic vortices.

1. Introduction

The phase diagram of finite isospin Quantum Chromodynamics (QCD) [1, 2] has generated significant interest in recent years with potential applications to the early universe [3] and heavy ion collisions, which is isospin asymmetric. Furthermore, there are predictions of exotic astrophysical objects such as pion stars [4, 5, 6] that is expected to form in supernovae remnants with the high neutrino density being the driving force that leads to the condensation of pions [7] in compact objects. Finite isospin QCD has the advantage of being accessible analytically at both low and asymptotically large isospin densities. At low densities, chiral perturbation theory (χ PT) [1, 2] or equivalently the nonlinear sigma model [8] shows the existence of a Bose-Einstein condensate and a superfluid and at asymptotically large isospin densities, the system has been shown to be a Bardeen-Cooper-Schrieffer (BCS) phase using high density effective theory [9, 10, 11] with the results being model-independent. Since finite isospin lattice QCD [12, 13] does not suffer from a sign problem, intermediate densities have also been studied with results in the low and high density regimes consistent with analytical results with future searches focusing on a possible crossover transition from the BEC to the BCS phase. For a review of finite isospin QCD, see

Ref. [14] and references therein including model dependent studies [15, 16].

The dynamics of the early universe and heavy ion collisions both occur in a magnetic field background suggesting that it is meaningful to explore the effect of the background on the phase diagram of finite isospin QCD. However, due to the asymmetry in the magnitude of the electromagnetic charges of the up and down quarks, the simultaneous presence of isospin and magnetic field introduces a sign problem to lattice QCD. Fortunately, due to the model-independent nature of χ PT, it is possible to map out the phase diagram of QCD at finite isospin density and a magnetic background in a regime where μ_I and \sqrt{eH} are both small compared to the typical hadronic scale ($\Lambda_{\text{Had}} \sim 4\pi f_\pi$), where f_π is the pion decay constant. In particular, there are two competing phases: in the absence of an anomaly, the charged pion superfluid that forms for isospin chemical potentials (μ_I) larger than the pion mass (m_π) behaves as an extreme type-II superconductor in a magnetic background for realistic physical parameters with the phase diagram allowing for either a single vortex near a lower critical magnetic field (H_{c1}), a magnetic vortex lattice below an upper critical magnetic field (H_{c2}) or a normal phase above the upper critical field, for $\mu_I > m_\pi$ which would support a superfluid pionic phase in the absence of a magnetic background [17, 18]. In the presence of an anomaly, however, finite isospin χ PT supports a neutral pion soliton lattice [19, 20], which is conjectured using a model-dependent version of χ PT to be the dominant

Email addresses: adhika1@stolaf.edu (Prabal Adhikari), leeser1@stolaf.edu (Elizabeth Leeser), markow2@stolaf.edu (Jake Markowski)

phase for isospin chemical potentials larger than approximately 500 MeV and magnetic fields (H) larger than 0.8 GeV² [21].

In this paper, we add to the emerging picture of the phase diagram of finite isospin QCD by studying the phonon modes associated with the triangular magnetic vortex lattice below and near the upper critical magnetic field [18]. In particular, we find the dispersion relations of the two acoustic and two optical modes by considering the quasimomentum fluctuations of the ground state in the lowest Landau level approximation (LLL). We find that one of the optical modes is massless with a dispersion relation that is quintic for small quasimomenta. We discuss the implications of this result for the phase diagram of finite isospin QCD including the possibility of magnetic vortices existing in a disordered (liquid/gas) phase.

The paper is organized as follows: we begin with a brief review of superfluidity in finite isospin χ PT in Section 2 followed by a review of the origin of superconductivity in Section 2.2. In Section 3, we introduce quasimomentum modes to the magnetic vortex solution in the LLL approximation. We then find the contribution to the potential and kinetic energies quadratic in the quasimomentum modes and find the dispersion relation of the acoustic and optical modes. Finally, we conclude in Section 4, with a discussion of possible scenarios for the phase diagram of the finite isospin QCD supporting magnetic vortices existing not only in an ordered (solid) phase but also a disordered (liquid/gas) phase.

2. Lagrangian and the origin of superconductivity

2.1. Lagrangian

We begin with the $\mathcal{O}(p^2)$ χ PT Lagrangian

$$\begin{aligned} \mathcal{L}_2 = & -\frac{1}{4}F_{\mu\nu}F^{\mu\nu} + \frac{f_\pi^2}{4}\text{Tr}[\nabla_\mu\Sigma(\nabla^\mu\Sigma)^\dagger] \\ & + \frac{f_\pi^2 m_\pi^2}{4}\text{Tr}[\Sigma + \Sigma^\dagger], \end{aligned} \quad (1)$$

where Σ is an $SU(2)$ matrix, f_π is the pion decay constant, m_π is the pion mass and $F_{\mu\nu} \equiv \partial_\mu A_\nu - \partial_\nu A_\mu$ is the electromagnetic tensor and $\nabla_\mu\Sigma$ is the covariant derivative. Their definitions are as follows

$$\nabla_\mu\Sigma = \partial_\mu\Sigma - i[eQA_\mu + \frac{\mu_l}{2}\tau_3\delta_{\mu 0}, \Sigma], \quad (2)$$

where A_μ is the electromagnetic gauge potential, $Q = \text{diag}(\frac{2}{3}, -\frac{1}{3})$ is the quark charge matrix and μ_l is the isospin chemical potential. In the two-flavor case, it is most convenient to parameterize the homogeneous ground state represented by the $SU(2)$ field, Σ , as

$$\Sigma = \cos\rho \mathbb{1} + \sin\rho i\hat{\phi}_a \tau_a, \quad (3)$$

where we have adopted the Einstein summation convention over repeated Greek indices, which represent isospin space. We require that $\hat{\phi}_a\hat{\phi}_a = 1$, which ensures the $SU(2)$ field Σ is unitary, i.e. $\Sigma^\dagger\Sigma = \mathbb{1}$. The resulting tree-level Lagrangian in the presence of an isospin chemical potential is

$$\mathcal{L}_{\text{tree}} = \frac{f_\pi^2 m_\pi^2}{2} \left[2\cos\rho + \sin^2\rho \left\{ \frac{\mu_l^2}{m_\pi^2} (\hat{\phi}_1^2 + \hat{\phi}_2^2) \right\} \right], \quad (4)$$

where setting $\hat{\phi}_1^2 + \hat{\phi}_2^2 = 1$ in the vacuum maximizes the tree-level Lagrangian, and also implies that $\hat{\phi}_3 = 0$, i.e. the neutral pion doesn't condense. Then maximizing the Lagrangian with respect to ρ , we find that the system possesses a normal vacuum with $\rho = 0$ when $|\mu_l| \leq m_\pi$ and charged pion phase with $\rho = \arccos\left(\frac{m_\pi^2}{\mu_l^2}\right)$ for $|\mu_l| \geq m_\pi$.

2.2. Origin of superconductivity

In order to study the superconducting characteristics of the pion condensed phase within finite isospin χ PT, we need the Gibbs free energy (density), which is the Legendre transform of the Hamiltonian (density), \mathcal{H} ,

$$\mathcal{G} = \mathcal{H} - \vec{M} \cdot \vec{H}. \quad (5)$$

where \vec{M} is the magnetization, which is defined as

$$\vec{M} = \vec{B} - \vec{H}. \quad (6)$$

Here $\vec{B} = \vec{\nabla} \times \vec{A}$, and \vec{H} is the external magnetic field, which we will assume points in the positive z -direction. Since charged superfluids behave superconductors we proceed by first stating the critical external magnetic field under the assumption of type-I superconductivity, which can be easily calculated by setting the Gibbs free energy of the uniform superconducting phase to that of the normal phase. In the superconductor, $\vec{B} = 0$ or equivalently $\vec{M} = -\vec{H}$. After setting the Gibbs free energy of the normal and superconducting phases, we find

$$H_c = \frac{f_\pi}{\mu_l} (\mu_l^2 - m_\pi^2). \quad (7)$$

On the other hand, assuming type-II superconductivity, there are two critical magnetic fields, the lower one, H_{c1} , determines the transition from the uniform superconducting phase to a single vortex phase and the higher one, H_{c2} determines the transition from a magnetic vortex lattice phase to the normal QCD vacuum. The lower critical field is

$$H_{c1} = \frac{\mathcal{S}}{\Phi}, \quad (8)$$

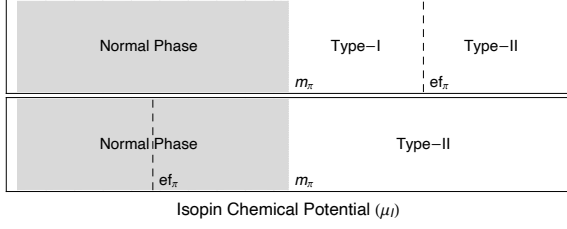


Figure 1: Phase diagram illustrating the nature of superconductivity in finite isospin χ PT. Top. $ef_\pi > m_\pi$: Both type-I and type-II superconductivity are supported for $\mu_I < ef_\pi$ and $\mu_I > ef_\pi$ respectively. Bottom. $ef_\pi < m_\pi$: Only type-II superconductivity is supported.

where \mathcal{S} is the string tension of a single magnetic vortex and Φ is the magnetic flux, which is quantized in the vortex. On the other hand, the upper critical field,

$$H_{c2} \equiv B_c = \frac{\mu_I^2 - m_\pi^2}{e}. \quad (9)$$

It is useful to note that H_c under the assumption of type-I and H_{c2} under the assumption of type-II are both proportional to $\mu_I^2 - m_\pi^2$ and satisfy

$$\mathcal{R} \equiv \frac{H_{c2}}{H_c} = \frac{\mu_I}{ef_\pi}, \quad (10)$$

which provides useful constraints on the values of physical parameters that determine the nature of superconductivity. The system behaves as a type-II superconductor if $\mathcal{R} > 1$, which in combination with the requirement that $\mu_I > m_\pi$ for the superfluid phase gives rise to the condition that if $ef_\pi < m_\pi$, the system only supports type-II superconductivity. However, if $ef_\pi > m_\pi$, the system exhibits both type-I and type-II superconductivity for $\mu_I < ef_\pi$ and $\mu_I > ef_\pi$ respectively. We illustrate these possibilities in Fig. 1.

3. Phonon modes

Before introducing quasimomentum fluctuations to the triangular magnetic vortex lattice that forms near the upper critical point and studying phonon dispersion relations, we briefly review the calculation of the vortex condensation energy first studied in Ref. [18]. Firstly, it is useful to expand the χ PT Lagrangian up to four fields

$$\begin{aligned} \mathcal{L}_{4\pi} = & -\frac{1}{4}F^{\mu\nu}F_{\mu\nu} + i\mu_I(\pi^- \partial_0 \pi^+ - \pi^+ \partial_0 \pi^-) \\ & - i\frac{2\mu_I}{3f_\pi^2}\pi^+\pi^-(\pi^-\partial_0\pi^+ - \pi^+\partial_0\pi^-) \\ & + D_\mu\pi^+D^\mu\pi^- + (\mu_I^2 - m_\pi^2)\pi^+\pi^- \\ & - \frac{4\mu_I^2 - m_\pi^2}{6f_\pi^2}(\pi^+\pi^-)^2 - \frac{1}{3f_\pi^2}D_\mu\pi^+D^\mu\pi^-\pi^+\pi^- \\ & + \frac{1}{6f_\pi^2}[\pi^+D_\mu\pi^-\pi^+D^\mu\pi^- + D_\mu\pi^+\pi^-D^\mu\pi^+\pi^-], \end{aligned} \quad (11)$$

which excludes a gauge-fixing term that is not necessary for a tree-level calculation and a trivial constant term ($f_\pi^2 m_\pi^2$). The covariant derivative $D_\mu \pi^\pm = (\partial_\mu + ieA_\mu)\pi^\pm$.

3.1. Method of successive approximation

Then we use the method of successive approximation to find the condensation energy and phonon modes of the magnetic vortex lattice. The approximation follows the following power counting scheme

$$B = B_0 + \varepsilon^2 \delta B \quad (12)$$

$$\pi^+ = \varepsilon \tilde{\pi}^+ + \varepsilon^3 \delta \pi^+, \quad (13)$$

where at leading order B_0 is the critical magnetic field B_c of Eq. (9) with $\tilde{\pi}^+$ obeying the following linearized equation of motion

$$\left(2\bar{\partial} + \frac{eB_0}{2}z\right)\tilde{\pi}^+ = 0, \quad (14)$$

where we have used ‘‘conformal’’ coordinates, i.e.

$$z = x + iy, \quad \bar{z} = x - iy \quad (15)$$

$$\partial = \frac{1}{2}(\partial_x - i\partial_y), \quad \bar{\partial} = \frac{1}{2}(\partial_x + i\partial_y). \quad (16)$$

The equation of motion for B upto $\mathcal{O}(\varepsilon^3)$ is

$$\bar{\partial}B = -e\bar{\partial}(\tilde{\pi}^+\tilde{\pi}^-) \left[1 - \frac{2}{3f_\pi^2}\tilde{\pi}^+\tilde{\pi}^-\right],$$

which has the following solution that incorporates magnetic flux conservation

$$\begin{aligned} B = & B_{\text{ext}} - e(\tilde{\pi}^+\tilde{\pi}^- - \langle\tilde{\pi}^+\tilde{\pi}^-\rangle) \\ & + \frac{e}{3f_\pi^2}((\tilde{\pi}^+\tilde{\pi}^-)^2 - \langle(\tilde{\pi}^+\tilde{\pi}^-)^2\rangle), \end{aligned} \quad (17)$$

with $\langle\mathcal{O}\rangle$ representing the expectation value of \mathcal{O} over the transverse plane, i.e.

$$\langle\mathcal{O}\rangle = \frac{1}{A_\perp} \int dx dy \mathcal{O}, \quad (18)$$

where A_\perp is the transverse area over which the integral is performed. Using the equations of motion then we can find the condensation energy, \mathcal{E}_\perp , of the magnetic vortex lattice relative to the normal vacuum. Using the definition,

$$\mathcal{E}_\perp \equiv \langle\mathcal{H}\rangle - \frac{1}{2}B_{\text{ext}}^2, \quad (19)$$

and the equations of motion we get the following condensation energy [18]

$$\begin{aligned} \mathcal{E}_\perp = & -e(B_c - B_{\text{ext}})\langle\tilde{\pi}^+\tilde{\pi}^-\rangle + \frac{e^2}{2}\langle\tilde{\pi}^+\tilde{\pi}^-\rangle^2 \\ & + \frac{1}{2}(\lambda_{\text{eff}} - e^2)\langle(\tilde{\pi}^+\tilde{\pi}^-)^2\rangle, \end{aligned} \quad (20)$$

where λ_{eff} is defined as

$$\lambda_{\text{eff}} \equiv \frac{2\mu_I^2 + m_\pi^2}{3f_\pi^2}. \quad (21)$$

The condensation energy is minimized by a triangular magnetic vortex lattice. The analytic form of the solution is

$$\tilde{\pi}^+ = \sum_{n=-\infty}^{\infty} C_n \phi_n(\mathbf{v}, z, \bar{z}) \quad (22)$$

$$\phi_n(\mathbf{v}, z, \bar{z}) = e^{-\pi v^2 n^2 - \frac{\pi}{2L_B^2}(|z|^2 + z^2) + \frac{2\pi}{L_B} v n z}, \quad (23)$$

where $L_B = \sqrt{\frac{2\pi}{eB}}$ is the magnetic length. For a triangular lattice that minimizes the free energy, $C_n = C_{n+2}$ with $C_0 \equiv C$, $C_1 = iC$ and $\mathbf{v} = \frac{\sqrt{3}}{2}\hat{z}$.

In order to calculate the transverse energy, we minimize Eq. (20) without the quasimomentum fluctuations we find that $\mathcal{E}_\perp^{(0)}$ is

$$\mathcal{E}_\perp^{(0)} = -\frac{e^2(B_c - B_{\text{ext}})^2}{2[e^2 + \beta_A(\lambda_{\text{eff}} - e^2)]}, \quad (24)$$

with corrections of $\mathcal{O}((B_c - B_{\text{ext}})^4)$ and the vortex lattice solution $\tilde{\pi}^+$ of Eq. (22) has

$$|C| = \sqrt{\frac{1}{Q_0} \frac{e(B_c - B_{\text{ext}})}{\beta_A(\lambda_{\text{eff}} - e^2) + e^2}}, \quad (25)$$

with $eB_c = \mu_I^2 - m_\pi^2 > 0$ and the Abrikosov ratio, $\beta_A = 1.159595\dots$.

3.2. Quasimomentum Excitations

In order to study the fluctuations of the vortex lattice, we introduce states that carry quasimomentum, \vec{k} , associated with the low-energy excitations of the magnetic vortex lattice [22, 23],

$$\tilde{\pi}_k^+(\vec{x}, t) = e^{-i(\vec{k}\cdot\vec{x} - \omega t)} \tilde{\pi}^+(\mathbf{x} + \frac{L_B^2}{\pi} \vec{k}), \quad (26)$$

where $\vec{x}(\vec{k})$ and $\mathbf{x}(\mathbf{k})$ represent position (quasimomentum) and traverse position (quasimomentum) respectively. Explicitly, $\vec{x} = (x, \mathfrak{z})$ and $\vec{k} = (\mathbf{k}, k_3)$ with $\mathbf{x} = (x, y)$ and $\mathbf{k} = (k_x, k_y)$. $\vec{\mathbf{k}}$ is defined as $\vec{\mathbf{k}}_i = \varepsilon_{ij} \mathbf{k}_j$, where ε_{ij} is the antisymmetric tensor, i.e. $\varepsilon_{12} = -\varepsilon_{21} = 1$. Finally, we note that the traverse quasimomenta live within a Brillouin zone, which is hexagonal, see Fig. 2 in Ref. [22].

The state that incorporates the quasimomentum excitations, $\tilde{\pi}_k^+(\vec{x}, 0)$, is a solution of the leading order equation of motion in Eq. (14), which is satisfied by the static magnetic vortex lattice. In order to incorporate the quasimomentum fluctuations of the magnetic vortex lattice, we proceed by expanding $\tilde{\pi}^\pm$ around the triangular vortex lattice as [23]

$$\tilde{\pi}^+(\mathbf{x}) \rightarrow \tilde{\pi}_k^+(\vec{x}) \equiv \tilde{\pi}_0^+(\mathbf{x}) + \chi^\dagger(\vec{x}, t) \quad (27)$$

$$\tilde{\pi}^-(\mathbf{x}) \rightarrow \tilde{\pi}_k^-(\vec{x}) \equiv \tilde{\pi}_0^-(\mathbf{x}) + \chi(\vec{x}, t), \quad (28)$$

where $\tilde{\pi}_0^\pm(\mathbf{x})$ represents the static triangular vortex lattice solution, with $\chi^\dagger(\vec{x}, t)$ and $\chi(\vec{x}, t)$ representing quasimomentum fluctuations around the triangular vortex lattice,

$$\chi^\dagger(\vec{x}, t) = \sum_{k \neq 0} c_k^\dagger \tilde{\pi}_k^+(\vec{x}, t). \quad (29)$$

The coefficient, c_k^\dagger , is complex-valued and represents small quasimomentum excitations, i.e. $|c_k^\dagger| \ll 1$.

In order to derive the phonon dispersion relations we require the effective phonon action of the magnetic vortex lattice that is quadratic in the fluctuations, i.e. c_k and/or c_k^\dagger ,

$$\mathcal{S}_{\text{phonon}}^{(2)} = \sum_{k \neq 0} \left(\mathcal{I}^{(2)}(k) - \mathcal{E}^{(2)}(k) \right), \quad (30)$$

where $\mathcal{I}^{(2)}(k)$ is the quadratic contribution arising from the time-dependent terms in Eq. (11) while $\mathcal{E}^{(2)}(k)$ is the potential energy contribution consisting of traverse and longitudinal contributions,

$$\mathcal{E}^{(2)}(k) \equiv \mathcal{E}_\perp^{(2)}(\mathbf{k}, 0) + \mathcal{E}_\parallel^{(2)}(\mathbf{0}, k_3). \quad (31)$$

The former will be calculated using Eq. (20) while the latter using Eq. (11). The quadratic contributions will then contain the following two-point function

$$\langle \tilde{\pi}_k^+ \tilde{\pi}_1^- \rangle = |C|^2 Q_0 \delta(\mathbf{k} - \mathbf{1}), \quad (32)$$

where $Q_0 \equiv \frac{1}{\sqrt{2}v}$ and the following four-point function (with only two non-zero quasimomenta), which is defined as

$$\langle \tilde{\pi}_{\mathbf{k}_2}^+ \tilde{\pi}_{\mathbf{k}_1}^- \tilde{\pi}_{\mathbf{k}_1}^+ \tilde{\pi}_{\mathbf{k}_2}^- \rangle \equiv |C|^4 Q_{\mathbf{k}_2 \mathbf{l}_2 \mathbf{k}_1 \mathbf{l}_1}. \quad (33)$$

$Q_{\mathbf{k}_2 \mathbf{l}_2 \mathbf{k}_1 \mathbf{l}_1}$ is real, dimensionless and symmetric under the following quasimomenta exchanges

$$Q_{\mathbf{k}_2 \mathbf{l}_2 \mathbf{k}_1 \mathbf{l}_1} = Q_{\mathbf{l}_2 \mathbf{k}_2 \mathbf{l}_1 \mathbf{k}_1}. \quad (34)$$

For our calculation of the effective phonon action, which is quadratic in \mathbf{k} , it is also helpful to note that it conserves quasimomentum. Further details of the four-point functions discussed in Appendix A with detailed calculations found in Ref. [22].

3.3. Transverse Energy

The transverse energy that incorporates quadratic fluctuations can be found using Eq. (20) after making the replacements in Eqs. (27) and (28),

$$\begin{aligned} \mathcal{E}_\perp^{(2)} = & -e(B_c - B_{\text{ext}}) \langle \chi^\dagger \chi \rangle + e^2 \langle \chi^\dagger \chi \rangle \langle \tilde{\pi}_0^+ \tilde{\pi}_0^- \rangle \\ & + \frac{1}{2} (\lambda_{\text{eff}} - e^2) [\langle \chi^\dagger \chi \tilde{\pi}_0^+ \tilde{\pi}_0^- \rangle + \langle \tilde{\pi}_0^+ \tilde{\pi}_0^- \chi^\dagger \chi \rangle \\ & + \langle \chi^\dagger \tilde{\pi}_0^- \tilde{\pi}_0^+ \chi \rangle + \langle \tilde{\pi}_0^+ \chi \chi^\dagger \tilde{\pi}_0^- \rangle \\ & + \langle \chi^\dagger \tilde{\pi}_0^- \chi^\dagger \tilde{\pi}_0^- \rangle + \langle \tilde{\pi}_0^+ \chi \tilde{\pi}_0^+ \chi \rangle], \end{aligned} \quad (35)$$

where we have used the orthogonality of the fluctuations to the static solution, i.e. $\langle \tilde{\pi}_0^- \chi \rangle = \langle \chi^\dagger \tilde{\pi}_0^+ \rangle = 0$. Since \mathcal{E}_\perp is strictly valid for static solutions with $k_3 = 0$, we replacing χ using Eq. (29) (after setting $k_3 = 0$). We get using Eq. (34) and quasimomentum conservation implicit in the four-point function [22],

$$\mathcal{E}_\perp^{(2)} = \sum_{\mathbf{k} \neq \mathbf{0}} \mathcal{E}_\perp^{(2)}(\mathbf{k}, 0) \quad (36)$$

$$\begin{aligned} \mathcal{E}_\perp^{(2)}(\mathbf{k}, 0) &= [-e(B_c - B_{\text{ext}})|C|^2 Q_0 + e^2|C|^4 Q_0^2 \\ &+ (\lambda_{\text{eff}} - e^2)|C|^4(Q_{\mathbf{k}\mathbf{k}\mathbf{0}\mathbf{0}} + Q_{\mathbf{k}\mathbf{0}\mathbf{0}\mathbf{k}})] c_{\mathbf{k}}^\dagger c_{\mathbf{k}} \quad (37) \\ &+ [(\lambda_{\text{eff}} - e^2)|C|^4 Q_{\mathbf{k}\mathbf{0}-\mathbf{k}\mathbf{0}}] \frac{1}{2}(c_{\mathbf{k}}^\dagger c_{-\mathbf{k}}^\dagger + c_{\mathbf{k}} c_{-\mathbf{k}}), \end{aligned}$$

where $Q_0 \equiv \frac{1}{\sqrt{2\nu}}$ and $c_{\mathbf{k}}$ represents the . The quadratic phonon Lagrangian is diagonal in the real representation of $c_{\mathbf{k}}^\dagger$,

$$c_{\mathbf{k}}^\dagger = o_{\mathbf{k}}^\dagger - i a_{\mathbf{k}}^\dagger, \quad c_{\mathbf{k}} = o_{\mathbf{k}} + i a_{\mathbf{k}}, \quad (38)$$

where $a_{\mathbf{k}}^\dagger$ and $o_{\mathbf{k}}^\dagger$ satisfy $a_{\mathbf{k}}^\dagger = a_{-\mathbf{k}}$, $o_{\mathbf{k}}^\dagger = o_{-\mathbf{k}}$, and

$$c_{\mathbf{k}}^\dagger c_{\mathbf{k}} = o_{\mathbf{k}}^2 + a_{\mathbf{k}}^2, \quad \frac{1}{2}(c_{\mathbf{k}}^\dagger c_{-\mathbf{k}}^\dagger + c_{\mathbf{k}} c_{-\mathbf{k}}) = o_{\mathbf{k}}^2 - a_{\mathbf{k}}^2. \quad (39)$$

The diagonal form of $\mathcal{E}_\perp^{(2)}(\mathbf{k}, 0)$ is

$$\begin{aligned} \mathcal{E}_\perp^{(2)}(\mathbf{k}, 0) &= \frac{1}{2}(\lambda_{\text{eff}} - e^2)|C|^4 [\lambda_-(\mathbf{k}) - \lambda_-(\mathbf{0})] o_{\mathbf{k}}^2 \\ &+ \frac{1}{2}(\lambda_{\text{eff}} - e^2)|C|^4 [\lambda_+(\mathbf{k}) - \lambda_-(\mathbf{0})] a_{\mathbf{k}}^2 \quad (40) \end{aligned}$$

where $\lambda_\pm(\mathbf{k})$ is defined as

$$\lambda_\pm(\mathbf{k}) \equiv 2(Q_{\mathbf{k}\mathbf{k}\mathbf{0}\mathbf{0}} + Q_{\mathbf{k}\mathbf{0}\mathbf{0}\mathbf{k}} \pm Q_{\mathbf{k}\mathbf{0}-\mathbf{k}\mathbf{0}}), \quad (41)$$

and $\lambda_-(\mathbf{0}) = 2Q_0^2 \beta_A$ in conjunction with Eq. (25) gives the compact form of $\mathcal{E}_\perp^{(2)}(\mathbf{k}, 0)$ in Eq. (40).

3.4. Longitudinal Energy

The contribution to the quadratic phonon Lagrangian of the longitudinal quasimomentum is most conveniently calculated using the derivative terms in Eq. (11) that depend on the longitudinal direction. We get

$$\mathcal{E}_\parallel^{(2)} = \mathcal{E}_{\parallel,0}^{(2)} + \mathcal{E}_{\parallel,d}^{(2)} = \sum_{k \neq 0} \left(\mathcal{E}_{\parallel,0}^{(2)}(k) + \mathcal{E}_{\parallel,d}^{(2)}(k) \right), \quad (42)$$

where the contribution due to the leading derivative term is $\mathcal{E}_{\parallel,0}^{(2)} = \langle \partial_3 \chi^\dagger \partial_3 \chi \rangle$, which gives

$$\mathcal{E}_{\parallel,0}^{(2)}(k) = k_3^2 |C|^2 Q_0 c_{\mathbf{k}}^\dagger c_{\mathbf{k}}. \quad (43)$$

The sub-leading derivative terms in $\mathcal{L}_{4\pi}$ contribute to

$$\begin{aligned} \mathcal{E}_{\parallel,d}^{(2)}(k) &= -k_3^2 |C|^4 \ell^2 \left[Q_{\mathbf{k}\mathbf{k}\mathbf{0}\mathbf{0}} c_{\mathbf{k}}^\dagger c_{\mathbf{k}} \right. \\ &\left. + Q_{\mathbf{k}\mathbf{0}-\mathbf{k}\mathbf{0}} \frac{1}{2}(c_{\mathbf{k}}^\dagger c_{-\mathbf{k}}^\dagger + c_{\mathbf{k}} c_{-\mathbf{k}}) \right], \quad (44) \end{aligned}$$

where $\ell \equiv \frac{1}{\sqrt{3}f_\pi}$. In terms of the real fields $o_{\mathbf{k}}$ and $a_{\mathbf{k}}$,

$$\begin{aligned} \mathcal{E}_\parallel^{(2)}(k) &= k_3^2 |C|^2 [Q_0 - |C|^2 \ell^2 \Lambda_+(\mathbf{k})] o_{\mathbf{k}}^2 \\ &+ k_3^2 |C|^2 [Q_0 - |C|^2 \ell^2 \Lambda_-(\mathbf{k})] a_{\mathbf{k}}^2, \quad (45) \end{aligned}$$

where $\Lambda_\pm(\mathbf{k}) = Q_{\mathbf{k}\mathbf{k}\mathbf{0}\mathbf{0}} \pm Q_{\mathbf{k}\mathbf{0}-\mathbf{k}\mathbf{0}}$.

3.5. Time-dependent contribution

The calculation of the time-dependent contribution of the quadratic phonon Lagrangian proceeds in a manner similar to the longitudinal (k_3 -dependent) contribution. However, as is evident from Eq. (11), there are also single time-derivative contributions proportional to the finite isospin chemical potential. We find

$$\begin{aligned} \mathcal{F}^{(2)} &= \mathcal{F}_0^{(2)} + \mathcal{F}_d^{(2)} \\ &= \sum_{k \neq 0} \left(\mathcal{F}_0^{(2)}(k) + \mathcal{F}_d^{(2)}(k) \right). \quad (46) \end{aligned}$$

where $\mathcal{F}_0^{(2)}$ is the contribution arising from the $\mathcal{O}(p^2)$ Lagrangian

$$\mathcal{F}_0^{(2)} = \langle \partial_0 \chi^\dagger \partial^0 \chi + i\mu_I (\partial_0 \chi^\dagger \chi - \chi^\dagger \partial_0 \chi) \rangle, \quad (47)$$

and

$$\mathcal{F}_0^{(2)}(k) = [\omega^2 - 2\mu_I \omega] |C|^2 Q_0 c_{\mathbf{k}}^\dagger c_{\mathbf{k}}. \quad (48)$$

$\mathcal{F}_d^{(2)}$ is the contribution arising from the $\mathcal{O}(p^4)$ derivative terms,

$$\begin{aligned} \mathcal{F}_d^{(2)} &= -2\ell^2 i\mu_I [\langle \tilde{\pi}_0^+ \tilde{\pi}_0^- (\partial_0 \chi^\dagger \chi - \chi^\dagger \partial_0 \chi) \rangle \\ &+ \langle \tilde{\pi}_0^+ \chi (\partial_0 \chi^\dagger \tilde{\pi}_0^- - \tilde{\pi}_0^+ \partial_0 \chi) \rangle \\ &+ \langle \chi^\dagger \tilde{\pi}_0^- (\partial_0 \chi^\dagger \tilde{\pi}_0^- - \tilde{\pi}_0^+ \partial_0 \chi) \rangle] \\ &- \ell^2 [\langle \tilde{\pi}_0^+ \tilde{\pi}_0^- \partial_0 \chi^\dagger \partial_0 \chi \rangle \\ &- \frac{1}{2} (\langle \tilde{\pi}_0^+ \partial_0 \chi \tilde{\pi}_0^+ \partial_0 \chi + \partial_0 \chi^\dagger \tilde{\pi}_0^- \partial_0 \chi^\dagger \tilde{\pi}_0^- \rangle)], \quad (49) \end{aligned}$$

and

$$\begin{aligned} \mathcal{F}_d^{(2)}(k) &= 4\ell^2 \mu_I \omega |C|^4 \left[(Q_{\mathbf{k}\mathbf{k}\mathbf{0}\mathbf{0}} + Q_{\mathbf{k}\mathbf{0}\mathbf{0}\mathbf{k}}) c_{\mathbf{k}}^\dagger c_{\mathbf{k}} \right. \\ &+ Q_{\mathbf{k}\mathbf{0}-\mathbf{k}\mathbf{0}} \frac{1}{2}(c_{\mathbf{k}}^\dagger c_{-\mathbf{k}}^\dagger + c_{\mathbf{k}} c_{-\mathbf{k}}) \left. \right] - \omega^2 \ell^2 |C|^4 \left[Q_{\mathbf{k}\mathbf{k}\mathbf{0}\mathbf{0}} c_{\mathbf{k}}^\dagger c_{\mathbf{k}} \right. \\ &+ Q_{\mathbf{k}\mathbf{0}-\mathbf{k}\mathbf{0}} \frac{1}{2}(c_{\mathbf{k}}^\dagger c_{-\mathbf{k}}^\dagger + c_{\mathbf{k}} c_{-\mathbf{k}}) \left. \right]. \quad (50) \end{aligned}$$

In terms of the real fields $o_{\mathbf{k}}$ and $a_{\mathbf{k}}$,

$$\begin{aligned} \mathcal{F}^{(2)} &= (\omega^2 - 2\mu_I \omega) |C|^2 [Q_0 - |C|^2 \ell^2 \Lambda_+(\mathbf{k})] o_{\mathbf{k}}^2 \\ &+ (\omega^2 - 2\mu_I \omega) |C|^2 [Q_0 - |C|^2 \ell^2 \Lambda_-(\mathbf{k})] a_{\mathbf{k}}^2 \\ &+ 2\ell^2 \mu_I \omega |C|^4 (\tilde{\Lambda}_+(\mathbf{k}) o_{\mathbf{k}}^2 + \tilde{\Lambda}_-(\mathbf{k}) a_{\mathbf{k}}^2), \quad (51) \end{aligned}$$

where $\tilde{\Lambda}_\pm(\mathbf{k}) = Q_{\mathbf{k}\mathbf{k}\mathbf{0}\mathbf{0}} + 2Q_{\mathbf{k}\mathbf{0}\mathbf{0}\mathbf{k}} \pm Q_{\mathbf{k}\mathbf{0}-\mathbf{k}\mathbf{0}}$.

3.6. Dispersion Relation

With the contributions to the quadratic action of Eq. (30) calculated, we can find the dispersion using the condition $\mathcal{F}^{(2)}(k) - \mathcal{E}^{(2)}(k) = 0$, which is equivalent to

$$(\omega^2 - 2\mu_I \omega) + 2\ell^2 \mu_I \omega g_\pm(\mathbf{k}) = k_3^2 + \tilde{h}_\pm(\mathbf{k}), \quad (52)$$

where $\tilde{h}_\pm(\mathbf{k}) = h_\pm(\mathbf{k})[\lambda_\mp(\mathbf{k}) - \lambda_-(\mathbf{0})]$ and

$$g_\pm(\mathbf{k}) = \frac{|C|^2}{Q_0} \tilde{\Lambda}_\pm(\mathbf{k}) \left(1 + \frac{|C|^2 \ell^2}{Q_0} \Lambda_\pm(\mathbf{k}) \right) \quad (53)$$

$$h_\pm(\mathbf{k}) = \frac{|C|^2}{2Q_0} (\lambda_{\text{eff}} - e^2) \left(1 + \frac{|C|^2 \ell^2}{Q_0} \Lambda_\pm(\mathbf{k}) \right). \quad (54)$$

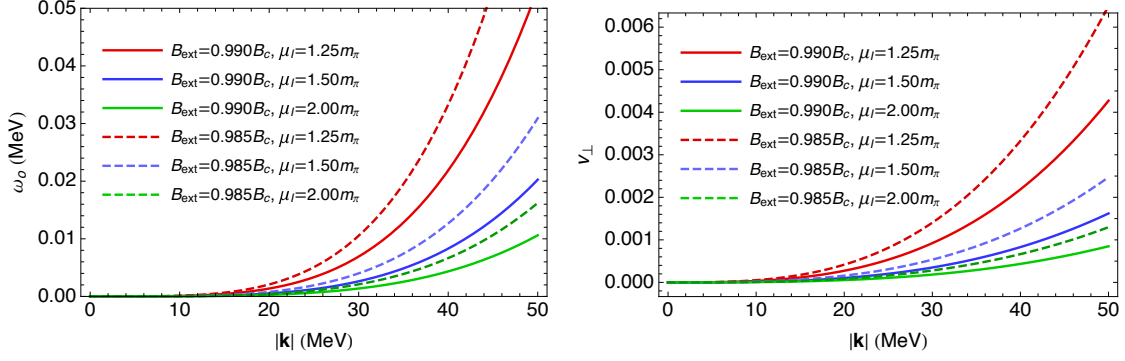


Figure 2: Plot of the dispersion relation associated with the massless optical mode (left) and its transverse velocity (right) as function of the transverse quasimomentum, $|\mathbf{k}|$. The solid and dashed lines represent the energy and speed at $B = 0.99B_c$ and $B = 0.985B_c$ respectively with the red, blue and green representing $\mu_I = 1.25m_\pi$, $1.50m_\pi$ and $1.75m_\pi$ respectively.

The resulting dispersion relations for the optical (ω_o) and the acoustic (ω_a) modes are

$$\omega_o(\mathbf{k}, k_3) = \mu_{I+}(\mathbf{k}) \pm \sqrt{k_3^2 + \mu_{I+}(\mathbf{k})^2 + \tilde{h}_+(\mathbf{k})} \quad (55)$$

$$\omega_a(\mathbf{k}, k_3) = \mu_{I-}(\mathbf{k}) \pm \sqrt{k_3^2 + \mu_{I-}(\mathbf{k})^2 + \tilde{h}_-(\mathbf{k})} \quad (56)$$

where $\mu_{I\pm}(\mathbf{k}) = \mu_I[1 - \ell^2 g_{\pm}(\mathbf{k})]$. Only one of the optical modes (ω_o) is massless since $\tilde{h}_+(\mathbf{0}) = 0$ but $\tilde{h}_-(\mathbf{0}) \neq 0$. For the massless mode, the dispersion relation for small transverse quasimomentum with $k_3 = 0$ is

$$|\omega_o(\mathbf{k}, 0)| = \frac{\alpha_4 h_+(\mathbf{0})}{|\mu_{I+}(\mathbf{0})|} \left(\frac{L_B \mathbf{k}}{\pi} \right)^4, \quad (57)$$

where $\alpha_4 \equiv 2(2q_4 - \tilde{q}_4) \approx 5.43$ and $h_+(\mathbf{0})$ is defined in Eq. (54) with $\Lambda_+(\mathbf{0}) = 2q_0 \approx 1.34$. q_i represent coefficients associated with the small quasimomentum expansion of the four-point functions discussed in Appendix in particular see Eqs. (A.7) and (A.8). The dispersion relation of the massless mode is softer than what one would expect in the absence of a chemical potential for which the dispersion relation is quadratic in the infrared limit [22, 24]. In the absence of a chemical potential ($\mu_I = 0$) and derivative interactions ($\ell = 0$), our result reduces to that of the Abelian Higgs model (assuming m_π^2 is negative): the massless mode in Eq. (55) is indeed quadratic for small \mathbf{k} and $k_3 = 0$.

On the left panel of Fig. 2, we plot the dispersion relation as a function of the transverse quasimomentum for small values of \mathbf{k} using $f_\pi = 93$ MeV and $m_\pi = 140$ MeV. We find that for a fixed magnetic field (relative to B_c) as the isospin chemical potential increases the energy of the massless mode decreases. Similarly, with an increase in the magnetic field (relative to B_c), the energy decreases. On the right panel of Fig. 2, we plot the speed of the massless mode in the transverse direction assuming $k_3 = 0$. Using the definition of the transverse speed, $\frac{\partial |\omega_o(\mathbf{k}, 0)|}{\partial \mathbf{k}}$, we find that for

small \mathbf{k} , it is up to $\mathcal{O}(\mathbf{k}^3 |C|^2)$

$$v_\perp = \frac{2\alpha_4 |C|^2 L_B^4 (\lambda_{\text{eff}} - e^2)}{Q_0 \pi^4 |\mu_+(\mathbf{0})|} |\mathbf{k}|^3 \quad (58)$$

with the expression valid for $\frac{L_B |\mathbf{k}|}{\pi} \ll 1$. We find that the transverse speed is approximately a factor of a thousand smaller than the speed of light. The speed decreases with increasing magnetic field and isospin chemical potential. Finally, we note that the speed of the massless mode in the longitudinal direction is $\frac{\partial |\omega_o(\mathbf{0}, k_3)|}{\partial k_3}$,

$$v_\parallel = \frac{|k_3|}{\sqrt{k_3^2 + \mu_{I+}(\mathbf{0})^2}}. \quad (59)$$

In contrast to the Abelian Higgs model, the longitudinal mode does not propagate at the the speed of light [22] it increases monotonically from zero to approximately 0.25 as the longitudinal momentum k_3 is increased from 0 MeV to 50 MeV and asymptotes to the speed of light for large k_3 . Similar to the transverse mode, the speed decreases with the increase of the isospin chemical potential and the increase of the magnetic field. However, the effect of the magnetic field is an order of magnitude weaker compared to the transverse mode since the only magnetic field dependence enters through $|\mu_{I+}(\mathbf{0})|$, see below Eq. (56).

4. Conclusion and implications for the phase diagram

In this paper, we have studied and characterized the dispersion relation of the phonon mode associated with the magnetic vortex lattice near the upper critical magnetic field in the LLL approximation. We find that the mode is proportional to \mathbf{k}^4 , which is softer than the ‘‘supersoft’’ modes observed in the Abelian Higgs Model [24]. The extreme supersoft nature of the phonon mode suggests that the vortex lattice can be easily perturbed away from their mean positions

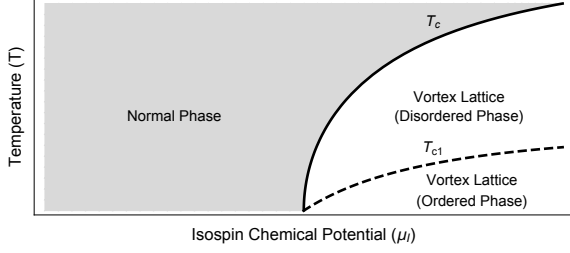


Figure 3: Schematic, finite temperature phase diagram illustrating a conjectured phase transition from an ordered to a disordered magnetic vortex phase with a melting temperature of T_{c1} .

and can exist in a disordered (“liquid” and/or “gas”) phase. Such a phase has been observed, for instance in lattice studies of the rho-condensed vacuum [25]. Unfortunately, lattice studies are not possible in finite isospin QCD in a magnetic background (with a dynamical gauge fields) due to the sign problem. However, it is possible to incorporate quantum effects using techniques similar to Ref [26] (where an ordered lattice was assumed): thermal fluctuations destroy the ordered magnetic vortex lattice in χ PT at a critical temperature of $T_c \sim f_\pi \sqrt{1 - m_\pi^2/\mu_I^2}$ [26]. Due to the extreme supersoft nature of the massless optical mode, it is conceivable that in addition to the transition at T_c , there is a further phase transition from an ordered magnetic vortex lattice to a disordered, liquid/gas phase unless incorporation of quantum effects and/or higher Landau levels [24] already destroys the ordered vortex lattice at zero temperature. In Fig. 3, we illustrate a possible finite temperature phase diagram of QCD with both ordered and disordered phases allowed. The critical temperature, T_{c1} , represents the transition from an ordered to a disordered phase unless the ordered phase is already destroyed by the inclusion of quantum effects at zero temperature. We conclude by noting that in the ordered phase, the phase diagram in the magnetic field-isospin chemical potential plane, is richer than traditionally depicted. In particular, we note the symmetries of a uniform superconductor, a single magnetic vortex and multiple vortices (including the vortex lattice)

$$\text{Superconductor: } \mathbb{R}_3 \times SO(3) \cong E(3) \quad (60)$$

$$\downarrow H \geq H_{c1}$$

$$\text{Single Vortex: } \mathbb{R}_3 \times SO(2)_{\theta+\alpha} \quad (61)$$

$$\downarrow H \geq H_{c3}$$

$$\text{Multiple Vortices: } \mathbb{R}_3 \times \emptyset, \quad (62)$$

where R_3 and $SO(3)$ represent translations and rotations (respectively) in three-dimensions, R_3 represents translation in the z -direction and $SO(2)_{\theta+\alpha}$ represents simultaneous physical and phase rotations of a single vortex, with the system being invariant if the angles are equal. Based on these symmetries there is an additional phase transition from a single vortex to a multi-

vortex phase, at H_{c3} that is traditionally omitted in literature perhaps because they share the same inhomogeneous order parameter.

Acknowledgements

P.A. would also like to thank Maxim Chernodub for helpful correspondence on quasimomentum states, and Andreas Schmitt for not only bringing Ref. [26] to our attention but also for a discussion of the critical temperature T_c in finite isospin χ PT. P.A. would also like to acknowledge Patrick Jefferson for helpful discussions on related issues. E.L. and J.M. would like to acknowledge the Collaborative Undergraduate Research and Inquiry (CURI) and Directed Undergraduate Research (DUR) programs for their support. Finally, P.A. acknowledges the support of St. Olaf startup funds.

Appendix A. Useful Mathematical Results: Four-Point Function

For notational convenience, we use the dimensionless quasimomentum $\bar{\mathbf{k}}$ and position $\bar{\mathbf{x}}$ throughout this appendix. They are defined as

$$\bar{\mathbf{k}} = \frac{L_B}{\pi} \mathbf{k}, \quad \bar{\mathbf{x}} = \frac{1}{L_B} \mathbf{x}, \quad (A.1)$$

where $L_B = \sqrt{\frac{2\pi}{eB_{\text{ext}}}}$ is the magnetic length. In terms of the dimensionless $\bar{\mathbf{x}}$ and $\bar{\mathbf{k}}$, the four-point function is defined as the transverse average – Eq. (18) – of the product of four pion fields with quasi-momenta,

$$\langle \tilde{\pi}_{\bar{\mathbf{k}}_2}^+ \tilde{\pi}_{\bar{\mathbf{k}}_1}^- \tilde{\pi}_{\bar{\mathbf{k}}_1}^+ \tilde{\pi}_{\bar{\mathbf{k}}_2}^- \rangle \equiv |C|^4 Q_{\bar{\mathbf{k}}_2 \bar{\mathbf{k}}_1 \bar{\mathbf{k}}_1 \bar{\mathbf{k}}_2}, \quad (A.2)$$

where $|C|$ has mass dimension one and $Q_{\bar{\mathbf{k}}_2 \bar{\mathbf{k}}_1 \bar{\mathbf{k}}_1 \bar{\mathbf{k}}_2}$ is dimensionless,

$$Q_{\bar{\mathbf{k}}_2 \bar{\mathbf{k}}_1 \bar{\mathbf{k}}_1 \bar{\mathbf{k}}_2} = Q_0^2 \sum_{m,n \in \mathbb{Z}} e^{-\pi(\mathbf{c} - \mathbf{X}_{m,n})^2 + 2\pi i \varepsilon_{ij} b^j X_{m,n}^i} \quad (A.3)$$

with $\mathbf{b} = \frac{\bar{\mathbf{k}}_1 + \bar{\mathbf{k}}_1 - \bar{\mathbf{k}}_2 - \bar{\mathbf{k}}_2}{2}$ and $\mathbf{c} = \frac{\bar{\mathbf{k}}_1 - \bar{\mathbf{k}}_1 - \bar{\mathbf{k}}_2 + \bar{\mathbf{k}}_2}{2}$. $\mathbf{X}_{m,n}$ is defined in terms of the lattice vectors \mathbf{d}_1 and \mathbf{d}_2 as

$$\mathbf{X}_{m,n} = (m\tilde{\mathbf{d}}_2 + n\tilde{\mathbf{d}}_1) = \frac{(m+n)v^{-1}}{2} \mathbf{e}_x - m v \mathbf{e}_y \quad (A.4)$$

where $\tilde{\mathbf{d}}_a = \frac{1}{L_B} \varepsilon_{ab} \mathbf{d}_b$, and \mathbf{e}_x and \mathbf{e}_y are unit vectors. For a detailed derivation of the four-point function in the symmetric gauge, see Ref. [22]. The lattice vectors associated with the triangular magnetic vortex lattice is

$$\mathbf{d}_1 = \frac{L_B}{v} \mathbf{e}_y, \quad \mathbf{d}_2 = \frac{L_B}{v} \left(\frac{\sqrt{3}}{2} \mathbf{e}_x + \frac{1}{2} \mathbf{e}_y \right) \quad (A.5)$$

where $v = \frac{1}{\sqrt{2}Q_0} = \frac{\sqrt{3}}{\sqrt{2}}$ for the triangular lattice. The four-point function is symmetric under the following non-trivial exchange of quasimomentum indices.

$$Q_{\bar{\mathbf{k}}_2 \bar{\mathbf{k}}_1 \bar{\mathbf{k}}_1 \bar{\mathbf{k}}_2} = Q_{\bar{\mathbf{k}}_2 \bar{\mathbf{k}}_1 \bar{\mathbf{k}}_1 \bar{\mathbf{k}}_2}. \quad (A.6)$$

This is in addition to trivial exchanges allowed by Eq. (18). The four-point correlation function holds only for small quasimomenta, $|\bar{k}_x| \leq \frac{\sqrt{2}Q_0}{4}$ and $|\bar{k}_y| \leq \frac{1}{2\sqrt{2}Q_0}$ [22]. We require the following small \mathbf{k} expansion of $Q_{\mathbf{k}\mathbf{k}\mathbf{0}\mathbf{0}}$, $Q_{\mathbf{k}\mathbf{0}\mathbf{0}\mathbf{k}}$ and $Q_{\mathbf{k}\mathbf{0}-\mathbf{k}\mathbf{0}}$ with only two non-zero momenta.

$$Q_{\mathbf{k}\mathbf{k}\mathbf{0}\mathbf{0}} = q_0 + q_2 \left(\frac{L_B}{\pi} \mathbf{k} \right)^2 + q_4 \left(\frac{L_B}{\pi} \mathbf{k} \right)^4 + \dots \quad (\text{A.7})$$

$$Q_{\mathbf{k}\mathbf{0}-\mathbf{k}\mathbf{0}} = q_0 + \tilde{q}_2 \left(\frac{L_B}{\pi} \mathbf{k} \right)^2 + \tilde{q}_4 \left(\frac{L_B}{\pi} \mathbf{k} \right)^4 + \dots \quad (\text{A.8})$$

where $Q_{\mathbf{k}\mathbf{k}\mathbf{0}\mathbf{0}} = Q_{\mathbf{k}\mathbf{0}\mathbf{0}\mathbf{k}}$ due to Eq. (A.2) and the coefficients are

$$q_0 = \frac{\beta_A}{2v^2} = 0.669493 \dots \quad (\text{A.9})$$

$$q_2 = -1.05164 \dots, \quad q_4 = 3.00957 \dots \quad (\text{A.10})$$

$$\tilde{q}_2 = -2.10327 \dots, \quad \tilde{q}_4 = 3.30381 \dots \quad (\text{A.11})$$

with $\tilde{q}_2 = 2q_2$.

References

- [1] D. T. Son and M. A. Stephanov, Phys. Rev. Lett. **86**, 592 (2001), arXiv:hep-ph/0005225 [hep-ph].
- [2] D. T. Son and M. A. Stephanov, Phys. Atom. Nucl. **64**, 834 (2001), [Yad. Fiz.64.899(2001)], arXiv:hep-ph/0011365 [hep-ph].
- [3] V. Vovchenko, B. B. Brandt, F. Cuteri, G. Endr3di, F. Hajkarim, and J. Schaffner-Bielich, Phys. Rev. Lett. **126**, 012701 (2021), arXiv:2009.02309 [hep-ph].
- [4] S. Carignano, L. Lepori, A. Mammarella, M. Mannarelli, and G. Pagliaroli, Eur. Phys. J. **A53**, 35 (2017), arXiv:1610.06097 [hep-ph].
- [5] B. B. Brandt, G. Endrodi, E. S. Fraga, M. Hippert, J. Schaffner-Bielich, and S. Schmalzbauer, (2018), arXiv:1802.06685 [hep-ph].
- [6] J. O. Andersen and P. Kneschke, (2018), arXiv:1807.08951 [hep-ph].
- [7] H. Abuki, T. Brauner, and H. J. Warringa, Eur. Phys. J. C **64**, 123 (2009), arXiv:0901.2477 [hep-ph].
- [8] R. Dashen and J. Manassah, Physics Letters A **47**, 453 (1974).
- [9] T. Kanazawa, T. Wettig, and N. Yamamoto, JHEP **12**, 007 (2011), arXiv:1110.5858 [hep-ph].
- [10] T. Kanazawa and T. Wettig, JHEP **10**, 055 (2014), arXiv:1406.6131 [hep-ph].
- [11] T. D. Cohen and S. Sen, Nucl. Phys. **A942**, 39 (2015), arXiv:1503.00006 [hep-ph].
- [12] J. B. Kogut and D. K. Sinclair, Phys. Rev. D **66**, 034505 (2002), arXiv:hep-lat/0202028.
- [13] B. B. Brandt, G. Endrodi, and S. Schmalzbauer, *Proceedings, 35th International Symposium on Lattice Field Theory (Lattice 2017): Granada, Spain, June 18-24, 2017*, EPJ Web Conf. **175**, 07020 (2018), arXiv:1709.10487 [hep-lat].
- [14] M. Mannarelli, Particles **2**, 411 (2019), arXiv:1908.02042 [hep-ph].
- [15] L. He and P. Zhuang, Phys. Lett. **B615**, 93 (2005), arXiv:hep-ph/0501024 [hep-ph].
- [16] P. Adhikari, J. O. Andersen, and P. Kneschke, Phys. Rev. **D98**, 074016 (2018), arXiv:1805.08599 [hep-ph].
- [17] P. Adhikari, T. D. Cohen, and J. Sakowitz, Phys. Rev. **C91**, 045202 (2015), arXiv:1501.02737 [nucl-th].
- [18] P. Adhikari, Phys. Lett. **B790**, 211 (2019), arXiv:1810.03663 [nucl-th].
- [19] T. Brauner and N. Yamamoto, JHEP **04**, 132 (2017), arXiv:1609.05213 [hep-ph].
- [20] T. Brauner, H. Koleřov3, and N. Yamamoto, Phys. Lett. B **823**, 136767 (2021), arXiv:2108.10044 [hep-ph].
- [21] M. S. Gr3nli and T. Brauner, (2022), arXiv:2201.07065 [hep-ph].
- [22] M. N. Chernodub, J. Van Doorselaere, and H. Verschelde, Phys. Rev. **D89**, 105011 (2014), arXiv:1401.0264 [hep-ph].
- [23] B. Rosenstein, Physical Review B **60**, 4268 (1999).
- [24] B. Rosenstein and D. Li, Rev. Mod. Phys. **82**, 109 (2010).
- [25] V. V. Braguta, P. V. Buividovich, M. Chernodub, M. I. Polikarpov, and A. Y. Kotov, PoS **ConfinementX**, 083 (2012), arXiv:1301.6590 [hep-lat].
- [26] A. Haber and A. Schmitt, Phys. Rev. **D95**, 116016 (2017), arXiv:1704.01575 [hep-th].